

# Giant Efficiency of Visible Second-Harmonic Light by an All-Dielectric Multiple-Quantum-Well Metasurface

Kun-Ching Shen<sup>ID</sup>,<sup>1</sup> Yi-Teng Huang<sup>ID</sup>,<sup>1</sup> Tsung Lin Chung,<sup>2</sup> Ming Lun Tseng,<sup>1</sup> Wei-Yi Tsai,<sup>1</sup> Greg Sun,<sup>4</sup> and Din Ping Tsai<sup>ID</sup><sup>1,2,3,\*</sup>

<sup>1</sup>Research Center for Applied Sciences, Academia Sinica, Taipei 11529, Taiwan

<sup>2</sup>Department of Physics, National Taiwan University, Taipei 10617, Taiwan

<sup>3</sup>Department of Electronic and Information Engineering, The Hong Kong Polytechnic University, Hung Hom, Kowloon, Hong Kong

<sup>4</sup>Department of Engineering, University of Massachusetts Boston, Massachusetts 02125, USA

(Received 23 April 2019; revised manuscript received 16 October 2019; published 26 December 2019)

Developing a high-efficiency coherent nonlinear light source is a critical step for photonic quantum technologies in signal processing, imaging, and switching. A promising approach is second-harmonic generation (SHG) via intersub-band transitions in a semiconductor quantum-well structure with a specific plasmon resonant mode of metal structures. There are, however, two significant challenges with this approach. First, limited by the conduction-band offset, the SHG wavelength based on intersub-band transitions is unlikely to extend into the visible region. Second, the high dissipative losses of plasmonic metal nanostructures could severely limit their applicability. Here we demonstrate an alternative configuration using interband excitonic transitions in an all-dielectric multiple-quantum-well metasurface capable of achieving high SHG conversion efficiency in the visible region. Taking advantage of the magnetic resonance of the multiple-quantum-well metasurface, the tightly concentrated optical field that is induced in the metasurface is responsible for boosting the conversion efficiency to about  $2 \times 10^{-7}$ . This demonstration opens a viable path toward a coherent light source using SHG that is extended to the visible region and beyond with high conversion efficiency, enabling nanophotonic quantum-information applications.

DOI: 10.1103/PhysRevApplied.12.064056

## I. INTRODUCTION

The conversion efficiency of second-harmonic generation (SHG) in metasurfaces can often be enhanced using the localized-surface-plasmon resonance of the periodic metal nanostructures [1–4]. This approach, however, suffers from a debilitating drawback owing to the huge metal loss in optical frequencies, rendering it impractical for all optical applications where efficiency is important. The inherently weak optical nonlinear processes could in theory be enhanced by the strong plasmonic fields induced by the metal nanostructures, but any potential efficiency boost would be completely offset by the large metal loss. Recent effort in metasurface development has therefore been shifted toward abolishing metals completely [5,6]. Metasurfaces made of all-dielectric units are engineered to possess electromagnetic responses in all four quadrants of the permittivity-permeability space without the devastating loss and are thus considered a promising alternative for a wide variety of applications, such as optical communications, biosensors, and energy conversion [7–9]. Recently,

all-dielectric metasurfaces with specific nanostructures supporting strong electric and magnetic Mie resonances have been shown to yield increased nonlinear conversion efficiencies [10–12]. However, many of these approaches suffer from self-absorption of the SHG signal by the dielectric media themselves because the photon energy of the signal is greater than the band gap. To solve this problem, SHG taking advantage of intersub-band transitions (ISTs) in multiple-quantum-well (MQW) structures that generate signal photon energy below the dielectric MQW band gap was proposed [13,14]. Differently from the all-dielectric MQWs embedded in metasurfaces (or metamaterials) as the gain medium to provide strong light-matter interaction enabled by their ultrasmall mode volume, which defies traditional diffractive optics and allows the demonstration of versatile control of the light wavefront and polarization [15–17], the case of ISTs in MQW structures capable of supporting larger second-order susceptibility  $\chi^{(2)}$  than conventional nonlinear materials achieves high-conversion efficiency for SHG for mid-IR and terahertz frequencies. Increase of the SHG conversion efficiency was indeed demonstrated by taking advantage of the enhanced  $\chi^{(2)}$  that is obtained by the plasmonic resonance

\*dptsai@phys.ntu.edu.tw

in metasurfaces with particular MQW configurations [18–20]. The large  $\chi^{(2)}$  is typically achieved near the frequency of the IST within the conduction band of a MQW structure. The conduction-band offsets in most semiconductor systems, however, limit such SHG processes to the mid-IR range or even a longer-wavelength range, putting near-IR and visible frequencies beyond reach. Another disadvantage associated with the SHG process based on plasmonic resonance near ISTs is the relatively high metal loss, severely hindering nonlinear applications for high-power excitations.

To extend the SHG response into the visible range and beyond, we explore optical nonlinearity in (In, Ga)N/GaN MQWs taking advantage of the interband excitonic transitions (IETs) associated with conduction and valence bands to enhance nonlinear light-matter interaction. There are several advantages with this interband approach. First, the SHG signal no longer suffers from the self-absorption of the dielectric medium because its photon energy is always equal to the effective band gap of the MQWs. Second, unlike for ISTs limited by conduction-band offset, a wider tuning range of the SHG-signal frequency is possible. Third, without metal nanostructures, the all-dielectric MQW metasurfaces are more compatible with current semiconductor technologies. In this study, we demonstrate high-efficiency SHG in the visible region using an all-dielectric (In, Ga)N/GaN MQW metasurface with a strong magnetic resonance that is carefully designed to deliver a strong SHG response near the interband transitions. The ultrathin MQW metasurface can produce a large second-order susceptibility  $\chi^{(2)}$  and a large SHG signal in a wide wavelength range with tuning of the MQW alloy compositions and layer thicknesses, establishing the foundation for tunable nonlinear optical devices.

## II. NONLINEAR BEHAVIORS IN THE MQW STRUCTURE

### A. Two-photon-excited photoluminescence and SHG

A three-pair (In, Ga)N/GaN MQW (well thickness 5 nm, barrier thickness 15 nm) with an indium content of 12% is prepared (see Sec. S1 in Supplemental Material [21]). Ti:sapphire-laser excitation in the 800–1050-nm wavelength range is used in conjunction with an electron-multiplying charge-coupled-device (EMCCD) camera and spectrometer (Princeton Instruments ProEM 512) to detect the spectrum and power of the SHG signal. Linearly polarized light from the pulsed laser passes through a 647-nm long-pass filter (EdgeBasic BLP01-647R-25) for wavelength purification. Then a near-IR objective with a numerical aperture of 0.4 (Mitutoyo Plan Apo  $\times 20$ ) and a visible objective with a numerical aperture of 0.95 (Nikon Plan Apo  $\times 60$ ) are used to focus the fundamental light to the sample and collect the SHG signal from the sample, respectively. A 647-nm short-pass filter (Semrock

SP01-633RU-25) is placed behind the visible objective to remove the fundamental pumping laser light. The optical setup in this study and the SHG results for an *n*-type GaN (*n*-GaN) control sample are presented in Supplemental Material (Figs. S2 and S3) [21].

The EMCCD camera is used to capture images spanning the fundamental to SHG frequency range as shown in Figs. 1(a) and 1(b). A bright spot is observed at around 450 nm in Fig. 1(a) for optical excitation at the pumping wavelength of 800 nm along with a long tail in the 420–600-nm wavelength range, which is attributed to the two-photon-excited photoluminescence (TPPL). Electron-hole pairs created by the absorption of two photons simultaneously at a wavelength of 800 nm subsequently recombine to emit photons of different wavelengths through a range of radiative recombination mechanisms associated with exciton, deep-state, and defect-state transitions in addition to nonradiative processes. The SHG signal at 400 nm is observed in Fig. 1(a). This signal is rather weak because photons at this wavelength can be reabsorbed directly by the MQW sample to generate electron-hole pairs inside the conduction and valence bands; these then go through similar recombination processes as those for TPPL. The log-log plot of the signal intensity at 450 nm versus the pumping power at the fundamental frequency (red curve) reveals a slope of 2.1 in Fig. 1(c), indicative of the involvement of the high-order nonlinear processes in TPPL [22]. In contrast, with increase of the pumping wavelength to 900 nm, carriers

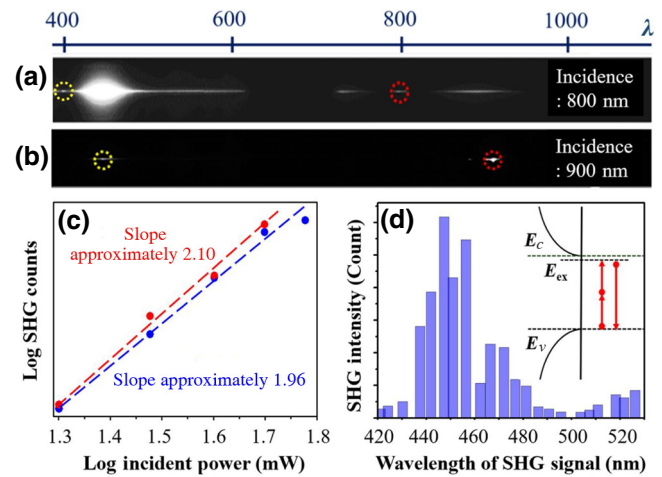


FIG. 1. (a),(b) EMCCD images of the planar MQW for incident wavelengths of 800 and 900 nm. Dotted red and yellow circles represent the wavelength locations of the pumping laser and the SHG signal, respectively. (c) Log-log plot of the signal intensity collected at a wavelength of 450 nm versus incident pumping power. (d) SHG intensity of the MQW at wavelengths between 840 and 1020 nm. The inset shows the dominant exciton transitions in the (In, Ga)N/GaN MQW. The band gap of the MQW is 2.80 eV and the exciton energy is about 40 meV below the conduction-band edge.

can no longer be excited by the two-photon-excitation process, and as a result only the SHG spot at 450 nm appears in Fig. 1(b). The relationship between the SHG intensity at 450 nm and the pumping power at 900 nm (blue curve) exhibits a slope of 1.96 in Fig. 1(c), a clear signature of a SHG process.

## B. IET mechanisms

To understand the transition mechanisms in MQWs responsible for the SHG response, we measure the SHG intensities of the sample by sweeping the pumping wavelength in the range from 840 to 1020 nm as shown in Fig. 1(d). In contrast to the monotonous SHG behavior over some spectral range for most conventional nonlinear materials, the SHG response in the MQW sample exhibits a strong wavelength dependence, where enhancement is observed at certain wavelengths. Such enhancement occurs around the exciton transition for the (In, Ga)N/GaN MQW sample. GaN-based materials possess large excitonic effects with strong oscillator strength. Its exciton binding energy has been determined to be around 40 meV below the band gap, and the wavelength of the exciton transition is around 450 nm [23,24]. As can be seen from Fig. 1(d), the strongest SHG signal is observed when its wavelength is near the resonance of the exciton transition as expected from the quantum-mechanical model [25] that predicts significant enhancement of second-order nonlinear susceptibility  $\chi^{(2)}$  as the SHG frequency approaches the band-gap transition in MQWs. In addition, SHG-signal enhancement is also observed throughout the broad blue-yellow spectral range, possibly due to the deep-level defect-state transitions [26,27]. To confirm these SHG responses are caused by the MQW, an *n*-GaN sample without MQWs is prepared as a control sample. Under

the same experimental condition, no SHG response is observed from this control sample, proving the nonlinear effects of the MQW directly.

The SHG conversion efficiency is determined by the ratio  $P_{2\omega}/P_\omega$ , where  $P_{2\omega}$  and  $P_\omega$  represent the SHG-signal power and the pumping power at the fundamental frequency, respectively. A maximum SHG conversion efficiency of  $6.2 \times 10^{-8}$  is found near the exciton transition at 450 nm, and  $\chi^{(2)}$  can be calculated according to the relation below between  $P_{2\omega}$  and  $P_\omega$  by [28]

$$P_{2\omega} = \frac{512\pi^4(\chi^{(2)})^2 L^2 P_\omega^2}{cn_\omega^2 n_{2\omega} d^2 \lambda^2}, \quad (1)$$

where  $L$  is the total MQW thickness,  $n_\omega$  and  $n_{2\omega}$  are the refractive indices at the pumping frequency and SHG frequency, respectively,  $d$  is the pumping-laser spot diameter,  $c$  is the speed of light in a vacuum, and  $\lambda$  is the pumping wavelength. According to Eq. (1), with the measured SHG-signal power  $P_{2\omega} = 3$  nW at the pumping power  $P_\omega = 40$  mW, we obtain  $\chi^{(2)} = 1.26 \times 10^{-10}$  m/V, which is 2 orders of magnitude higher than the value for bulk GaN (approximately  $10^{-12}$  m/V). This result provides clear evidence that the SHG response is dramatically enhanced when the SHG frequency is close to the resonance of IETs in the (In, Ga)N/GaN MQW structure, much like what has been demonstrated by the ISTs, extending the high-efficiency SHG process nicely into the visible range.

## III. DESIGN OF THE MQW METASURFACE

To further boost the SHG efficiency, the possibility of an additional enhancement induced by the resonance from structures is explored. We process the (In, Ga)N/GaN

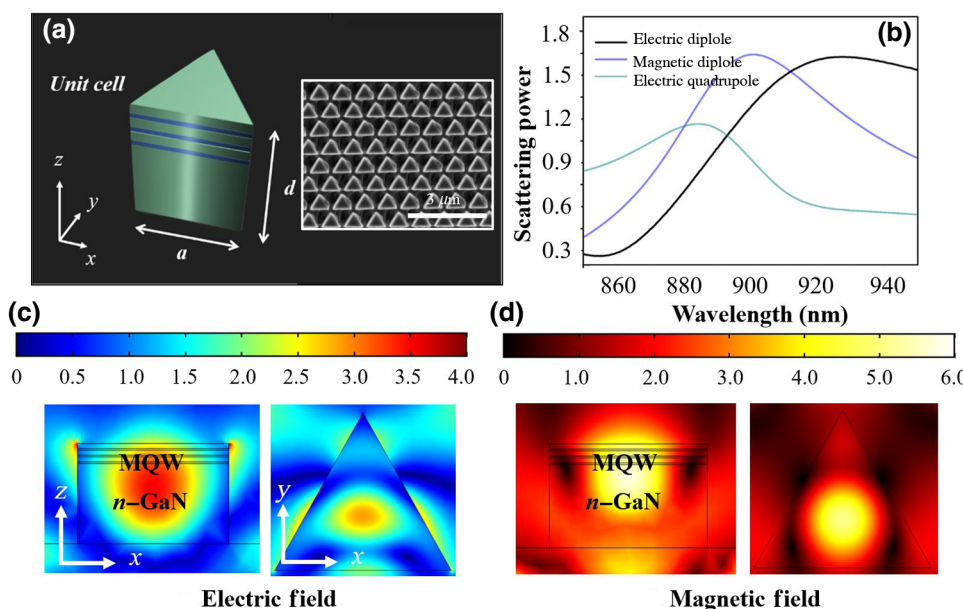


FIG. 2. (a) Unit cell of the MQW metasurface. The inset show a scanning-electron-microscopy image (oblique view) of the fabricated MQW metasurface. (b) Simulation result for the scattering power for electric dipole, magnetic dipole, and electric quadrupole modes. (c) Electric field and (d) magnetic field enhancement distributed on the  $x$ - $z$  plane and the  $x$ - $y$  plane for 900-nm incident light.

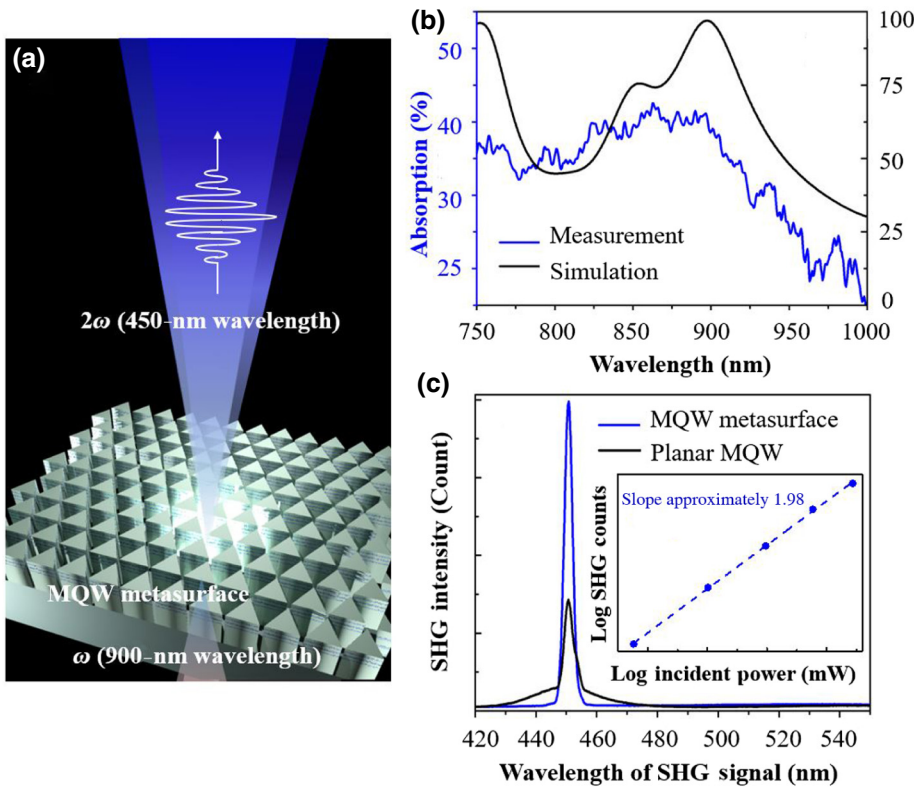


FIG. 3. (a) The nonlinear MQW metasurface. (b) Absorption spectrum of the experimental and simulation results. (c) SHG intensity of the MQW metasurface and planar MQW sample obtained with linearly polarized incident light. The inset shows the log-log curve of the MQW metasurface for a SHG signal of 450-nm wavelength.

MQWs into a metasurface to create a Mie resonance at a specific wavelength of the pumping laser. The metasurface pattern we implement here is an array composed of several triangular nanopillars [Fig. 2(a)], which has demonstrated efficient SHG conversion and polarization control in previous studies [29]. In our research, the finite-element method as implemented in COMSOL MULTIPHYSICS 5.3a is used to optimize the structural geometries and simulate the field distribution (see Figs. S4 and S5 in Supplemental Material [21]). Since the MQW shows the strongest SHG enhancement at 450 nm, we aim to achieve a resonance feature at a fundamental wavelength of 900 nm. The length of the equilateral side  $a$ , the nanopillar height  $d$ , and the period  $P$  of the metasurface are optimized to be 700, 300, and 830 nm, respectively. A MQW metasurface with an area of  $40 \times 40 \mu\text{m}^2$  is fabricated by a focused-ion-beam system (FEI Helios 660 NanoLab). A top-view scanning-electron-microscope image of the MQW metasurface is shown in the inset in Fig. 2(a). The simulated scattering powers of the electric dipole, magnetic dipole, and electric quadrupole modes induced inside the optimal structures are shown in Fig. 2(b) and in Fig. S6 in Supplemental Material [21]. Under the excitation of a linearly polarized pumping source ( $E_x$  or  $E_y$ ), a dominant magnetic dipole resonance can be seen to peak at 900 nm. Figures 2(c) and 2(d) show the electric and magnetic field distributions of the magnetic dipole mode at 900 nm, where a maximum enhancement of 3–4 times and 8–9 times, respectively, is

achieved. The enhancement of the effective second-order nonlinear-susceptibility tensor can also be theoretically calculated via the formula [18]

$$\chi_{ijk}^{(2)\text{eff}} = \frac{\int_V f^{2\omega}(x, y, z) f_{n(j)}^\omega(x, y, z) f_{p(k)}^\omega(x, y, z) dV}{\chi_{mnp}^{(2)} V}, \quad (2)$$

where  $\chi_{ijk}^{(2)\text{eff}}$  and  $\chi_{mnp}^{(2)}$  are the effective and intrinsic second-order nonlinear-susceptibility tensors of the material, respectively,  $f^{2\omega}$  and  $f^\omega$  are the field enhancement at the SHG frequency (wavelength 450 nm) and the fundamental frequency (wavelength 900 nm), respectively, and  $V$  is the volume of a unit nanopillar. The field enhancement  $f^\omega$  at the fundamental frequency is primarily responsible for the SHG enhancement because of the strong magnetic dipole resonance. The enhancement of both  $\chi_{xxx}^{(2)}$  and  $\chi_{yyy}^{(2)}$  is estimated to be 1.3 according to Eq. (2), and an induced electric field  $E_z$  also leads to efficient SHG conversion in the  $z$  direction as well. Eventually, this MQW metasurface is capable of enhancing the SHG efficiency in all three directions. In addition, although the enhanced field at the magnetic dipole mode extends into both the MQW and the n-GaN layer underneath, the SHG signal should originate mainly from the MQW part owing to its much stronger nonlinear response compared with that of the n-GaN part.

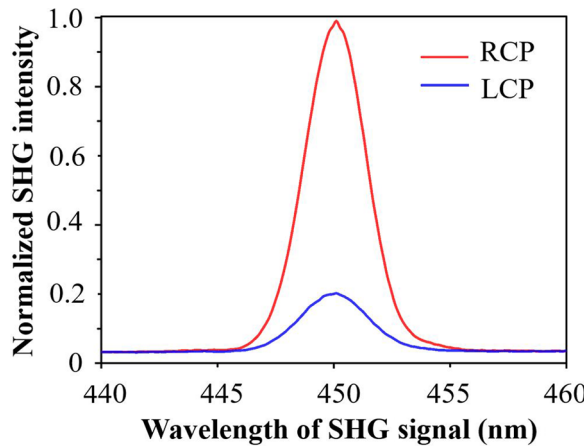


FIG. 4. RCP and LCP components of the SHG intensity collected with LCP incident light.

#### IV. RESULTS

The optical absorption of the MQW metasurface [Fig. 3(a)] is measured with a spectrometer (Olympus OLO7861), and its absorption spectrum is shown in Fig. 3(b). The measured spectrum is in good agreement with the simulated result, which has a stronger absorption around 900 nm. The discrepancy between the experimental and simulation results is likely due to the imperfection of the fabricated structures. In comparison with the planar MQW sample, the MQW metasurface shows a nearly 3 times enhancement of the SHG intensity when excited by the 900-nm pumping laser, as can be seen in Fig. 3(c). A slope of approximately 1.98 in the log-log plot [the inset in Fig. 3(c)] also confirms the occurrence of the SHG process in the MQW metasurface. The SHG conversion efficiency of the MQW metasurface is subsequently calculated, and a highest efficiency of approximately  $2 \times 10^{-7}$  is reached at a pumping power of 40 mW, and is about 3 times that of the planar MQW sample.

Additionally, the surface roughness of the metasurface structure might lead to SHG enhancement due to the field enhancement caused by its nanoscale feature [30]. To understand the effect of the surface roughness in our device, we measure the SHG intensities produced by the same MQW metasurface structure with a different ion-beam milling time. The average surface roughness is about 5 nm. These MQW metasurfaces show a decrease of SHG intensities with increase of the milling time because of the milling depth throughout the MQW region (i.e., part of MQW is removed). Only the one with an absorption peak at 900 nm demonstrates an obvious SHG enhancement. We thus claim that in our device, the SHG effect resulting from surface roughness might be relatively weak compared with that from Mie resonance.

It is worth noting that the triangular nanopillars of the MQW metasurface can also be used to control the SHG

polarization according to the selection rule, which applies when a circularly polarized fundamental wave propagates normally toward a structure with  $n$ -fold rotation symmetry [29,31]. As a result, the SHG signals produced from the triangular nanopillars under the excitation of left circularly polarized (LCP) light will be right circularly polarized (RCP) and vice versa because of the threefold rotational symmetry of the triangle. Figure 4 displays the RCP and LCP components of the SHG signal with LCP pumping at 900 nm. A RCP-to-LCP ratio of 5 can be seen in the experiment, showing that our device could serve as a coherent light source with controllable polarization, which is an essential tool for structural analysis of biomolecules [32,33].

#### V. CONCLUSION

In summary, the strong SHG enhancement near the band gap of the (In, Ga)N/GaN MQW is attributed to the large IET effect. With the use of IETs, the SHG frequencies are no longer limited by the conduction-band offset as are those based on ISTs. This is a major step forward in extending the SHG-signal frequency into the visible regime or beyond. The all-dielectric feature of the MQW reduces the concerns for metal loss and structure damage. Furthermore, we prove that even greater SHG enhancement could be achieved by fabricating a triangularly patterned MQW metasurface. A high SHG conversion efficiency of  $2 \times 10^{-7}$  is demonstrated at the SHG wavelength of 450 nm, which is a relatively challenging wavelength to achieve compared with IR wavelengths. This metasurface also exhibits the ability to control the polarization of the SHG signal in our experiment. With its high conversion efficiency and polarization-control feature, this MQW metasurface might have the potential to be a versatile nonlinear light source for numerous applications in quantum signal processing, imaging, or microscopy.

#### ACKNOWLEDGMENTS

The authors acknowledge financial support from Shenzhen Innovation Technology D-type Project, Grant No. SGDX2019081623281169 (2019), No. 274. The authors are also grateful to the Research Center for Applied Sciences, Academia Sinica, Taiwan, and the Department of Electronic and Information Engineering, The Hong Kong Polytechnic University, for their support. K.C.S. and Y.T.H. contributed equally to this work. K.C.S. and D.P.T. conceived the project. K.C.S. grew the (In, Ga)N/GaN MQW samples and performed the material investigation. Y.T.H. fabricated the metasurface. Y.T.H., M.L.T., and W.Y.T. performed numerical simulations. K.C.S., Y.T.H., and T.L.C. supported the optical measurements. K.C.S., Y.T.H., G.S., and D.P.T. analyzed the experimental data and wrote the manuscript. K.C.S. and D.P.T. supervised the

research. All authors discussed the results and commented on the manuscript.

- 
- [1] J. B. Khurgin and G. Sun, Plasmonic enhancement of the third order nonlinear optical phenomena: Figures of merit, *Opt. Express* **21**, 27460 (2013).
- [2] M. Celebrano, X. Wu, M. Baselli, S. Großmann, P. Biagioni, A. Locatelli, C. D. Angelis, G. Cerullo, R. Osellame, B. Hecht, L. Duò, F. Ciccacci, and M. Finazzi, Mode matching in multiresonant plasmonic nanoantennas for enhanced second harmonic generation, *Nat. Nanotechnol.* **10**, 412 (2015).
- [3] Y. Zhang, N. K. Grady, C. Ayala-Orozco, and N. J. Halas, Three-dimensional nanostructures as highly efficient generators of second harmonic light, *Nano Lett.* **11**, 5519 (2011).
- [4] W.-Y. Tsai, T. L. Chung, H.-H. Hsiao, J.-W. Chen, R. J. Lin, P. C. Wu, G. Sun, C.-M. Wang, H. Misawa, and D. P. Tsai, Second harmonic light manipulation with vertical split ring resonators, *Adv. Mater.* **31**, 1806479 (2018).
- [5] S. Jahani and Z. Jacob, All-dielectric metamaterials, *Nat. Nanotechnol.* **11**, 23 (2016).
- [6] G. Li, S. Zhang, and T. Zentgraf, Nonlinear photonic metasurfaces, *Nat. Rev. Mater.* **2**, 17010 (2017).
- [7] M. Kauranen and A. V. Zayats, Nonlinear plasmonics, *Nat. Photonics* **6**, 737 (2012).
- [8] A. Krasnok, M. Tymchenko, and A. Alu, Nonlinear metasurfaces: A paradigm shift in nonlinear optics, *Mater. Today* **21**, 8 (2018).
- [9] A. I. Kuznetsov, A. E. Miroshnichenko, M. L. Brongersma, Y. S. Kivshar, and B. Luk'yanchuk, Optically resonant dielectric nanostructures, *Science* **354**, 2472 (2016).
- [10] S. V. Makarov, M. I. Petrov, U. Zywicki, V. Milichko, D. Zuev, N. Lopanitsyna, A. Kuksin, I. Mukhin, G. Zografi, E. Ubyivovk, D. A. Smirnova, S. Starikov, B. N. Chichkov, and Y. S. Kivshar, Efficient second-harmonic generation in nanocrystalline silicon nanoparticles, *Nano Lett.* **17**, 3047 (2017).
- [11] M. Semmlinger, M. L. Tseng, J. Yang, M. Zhang, C. Zhang, W.-Y. Tsai, D. P. Tsai, P. Nordlander, and N. J. Halas, Vacuum ultraviolet light-generating metasurface, *Nano Lett.* **18**, 5738 (2018).
- [12] V. F. Gili, L. Carletti, A. Locatelli, D. Rocco, M. Finazzi, L. Ghirardini, I. Favero, C. Gomez, A. Lemaître, M. Celebrano, C. De Angelis, and G. Leo, Monolithic AlGaNAs second-harmonic nanoantennas, *Opt. Express* **24**, 15965 (2016).
- [13] K.-C. Shen, C. Hsieh, Y.-J. Cheng, and D. P. Tsai, Giant enhancement of emission efficiency and light directivity by using hyperbolic metacavity on deep-ultraviolet AlGaN emitter, *Nano Energy* **45**, 353 (2018).
- [14] K.-C. Shen, C.-T. Ku, C. Hsieh, H.-C. Kuo, Y.-J. Cheng, and D. P. Tsai, Deep-ultraviolet hyperbolic metacavity laser, *Adv. Mater.* **30**, 1706918 (2018).
- [15] E. Rosencher, A. Fiore, B. Vinter, V. Berger, Ph. Bois, and J. Nagle, Quantum engineering of optical nonlinearities, *Science* **271**, 168 (1996).
- [16] G. Serapiglia, E. Paspalakis, C. Sirtori, K. Vodopyanov, and C. Phillips, Laser-Induced Quantum Coherence in a Semiconductor Quantum Well, *Phys. Rev. Lett.* **84**, 1019 (2000).
- [17] J. Khurgin, Second-order nonlinear effects in asymmetric quantum-well structures, *Phys. Rev. B* **38**, 4056 (1988).
- [18] J. Lee, M. Tymchenko, C. Argyropoulos, P.-Y. Chen, F. Lu, F. Demmerle, G. Boehm, M.-C. Amann, A. Alù, and M. A. Belkin, Giant nonlinear response from plasmonic metasurfaces coupled to intersubband transitions, *Nature* **511**, 65 (2014).
- [19] O. Wolf, S. Campione, A. Benz, A. P. Ravikumar, S. Liu, T. S. Luk, E. A. Kadlec, E. A. Shaner, J. F. Klem, M. B. Sinclair, and I. Brener, Phased-array sources based on nonlinear metamaterial nanocavities, *Nat. Commun.* **6**, 7667 (2015).
- [20] O. Wolf, A. A. Allerman, X. Ma, J. R. Wendt, A. Y. Song, E. A. Shaner, and I. Brener, Enhanced optical nonlinearities in the near-infrared using III-nitride heterostructures coupled to metamaterials, *Appl. Phys. Lett.* **107**, 151108 (2015).
- [21] See Supplemental Material at <http://link.aps.org/supplemental/10.1103/PhysRevApplied.12.064056> for details of the experimental results for the n-GaN control sample, the simulated electric field distribution and field enhancement at the SHG frequency, and the scattering-power calculation.
- [22] J. Dai, J.-H. Zeng, S. Lan, X. Wan, and S.-L. Tie, Competition between second harmonic generation and two-photon-induced luminescence in single, double and multiple ZnO nanorods, *Opt. Express* **21**, 10025 (2013).
- [23] M. Dvorak, S.-H. Wei, and Z. Wu, Origin of the Variation of Exciton Binding Energy in Semiconductors, *Phys. Rev. Lett.* **110**, 016402 (2013).
- [24] S. Sankaranarayanan, S. Chouksey, P. Saha, V. Pendem, A. Udai, T. Aggarwal, S. Ganguly, and D. Saha, Determination of strain relaxation in InGaN/GaN nanowalls from quantum confinement and exciton binding energy dependent photoluminescence peak, *Sci. Rep.* **8**, 8404 (2018).
- [25] R. W. Boyd, *Nonlinear Optics* (Academic Press, New York, 2008).
- [26] W. Angerer, N. Yang, A. Yodh, M. Khan, and C. Sun, Ultrafast second-harmonic generation spectroscopy of GaN thin films on sapphire, *Phys. Rev. B* **59**, 2932 (1999).
- [27] Y. Toda, T. Matsubara, R. Morita, M. Yamashita, K. Hoshino, T. Someya, and Y. Arakawa, Two-photon absorption and multiphoton-induced photoluminescence of bulk GaN excited below the middle of the band gap, *Appl. Phys. Lett.* **82**, 4714 (2003).
- [28] F. Zernike and J. E. Midwinter, *Applied Nonlinear Optics* (Wiley, New York, 1967).
- [29] K. Konishi, T. Higuchi, J. Li, J. Larsson, S. Ishii, and M. Kuwata-Gonokami, Polarization-controlled Circular Second-Harmonic Generation From Metal Hole Arrays with Threefold Rotational Symmetry, *Phys. Rev. Lett.* **112**, 135502 (2014).
- [30] A. Wickberg, A. Abass, H.-H. Hsiao, C. Rockstuhl, and M. Wegener, Second-harmonic generation by 3D laminate metacrystals, *Adv. Opt. Mater.* **7**, 1801235 (2019).

- [31] S. Chen, G. Li, F. Zeuner, W. H. Wong, E. Y. B. Pun, T. Zentgraf, K. W. Cheah, and S. Zhang, Symmetry-Selective Third-Harmonic Generation From Plasmonic Metacrystals, *Phys. Rev. Lett.* **113**, 033901 (2014).
- [32] V. K. Valev, J. J. Baumberg, C. Sibilia, and T. Verbiest, Chirality and chiroptical effects in plasmonic nanostructures: Fundamentals, recent progress, and outlook, *Adv. Mater.* **25**, 2517 (2013).
- [33] G. Li, S. Chen, N. Pholchai, B. Reineke, P. W. H. Wong, E. Y. B. P. K, W. Cheah, T. Zentgraf, and S. Zhang, Continuous control of the nonlinearity phase for harmonic generations, *Nat. Mater.* **14**, 607 (2015).